

# Search for universal roughness distributions in a critical interface model

S.L.A. de Queiroz\*

*Instituto de Física, Universidade Federal do Rio de Janeiro,  
Caixa Postal 68528, 21941-972 Rio de Janeiro RJ, Brazil*

(Dated: 8th February 2020)

We study the probability distributions of interface roughness, sampled among successive equilibrium configurations of a single-interface model used for the description of Barkhausen noise in disordered magnets, in space dimensionalities  $d = 2$  and  $3$ . We attempt to fit our data to the class of roughness distributions associated to  $1/f^\alpha$  noise. The influence of a self-regulating (demagnetization) mechanism is investigated, and evidence is given to show that it is irrelevant, which implies that the model belongs to the Edwards-Wilkinson universality class. Periodic, free, and mixed boundary conditions are examined, with rather distinct results as regards quality of fits to  $1/f^\alpha$  distributions.

PACS numbers: 05.65.+b, 05.40.-a, 75.60.Ej, 05.70.Ln

## I. INTRODUCTION

This paper deals with fluctuation properties of driven interfaces in random media. The subject has been the focus of much current interest (for reviews see, e.g., Refs. 1, 2). Special attention has been given to features at and close to the depinning transition, where a threshold is reached for the external driving force, above which the interface starts moving at a finite speed. In analogy with the well-established scaling theory of equilibrium critical phenomena, one usually searches for the underlying universality classes and their respective critical indices, wherever such concepts are applicable. One example is the roughness exponent  $\zeta$  which characterizes the disorder-averaged mean-square deviations of the interface about its mean height, at depinning [1].

It has been shown very recently that the probability distribution functions (PDFs) of critical fluctuations in seemingly disparate (both equilibrium and out-of-equilibrium) systems display a remarkable degree of universality [3, 4, 5, 6]. In the context of depinning phenomena, this indicates that one may gain additional insight into the physical mechanisms involved, by investigating the full roughness PDFs instead of concentrating on their lowest-order moments. Here we investigate the PDFs of interface roughness for a specific single-interface model which has been used in the description of Barkhausen noise [7, 8, 9, 10], and is related to the quenched Edwards-Wilkinson universality class [11, 12, 13, 14]. A preliminary investigation of this problem was reported in Ref. 10.

Barkhausen “noise” (BN) is an intermittent phenomenon which reflects the dynamics of domain-wall motion in the central part of the hysteresis cycle in ferromagnetic materials (see Ref. 15 for an up-to-date review). A sample placed in a time-varying external magnetic field undergoes sudden microscopic realignments of groups of

magnetic moments, parallel to the field. For suitably slow driving rates, such domain-wall motions, or “avalanches”, are well separated and can be easily individualized. The accompanying changes of magnetic flux are usually detected by wrapping a coil around the sample and measuring the voltage pulses thus induced across the coil. The integral of the voltage amplitude of a given pulse over time is proportional to the change in sample magnetization, thus giving a measure of the number of spins overturned in that particular event, or “avalanche size”. Modern experimental techniques allow direct observation, in ultra-thin films, of the domain-wall motion characteristic of BN, via the magneto-optical Kerr effect [16, 17].

It has been proposed that BN is an illustration of “self-organized criticality” [7, 18, 19, 20], in the sense that a broad distribution of scales (i.e. avalanche sizes) is found within a wide range of variation of the external parameter, namely the applied magnetic field, without any fine-tuning. Accordingly, the interface model studied here incorporates a self-regulating mechanism in the form of a demagnetizing term (see below). In the context of interface depinning models, the question arises of whether this is a relevant perturbation, i.e., whether self-organized depinning phenomena belong to the same universality class as their counterparts which do not incorporate such mechanisms.

In what follows, we first recall pertinent aspects of the interface model used here, and of our calculational methods, as well as the connections between roughness distributions and  $1/f^\alpha$  noise. Next, we exhibit numerical data for roughness distributions, generated by our simulations. We examine the influence of the self-regulating mechanism, and investigate the effect of assorted boundary conditions, both on our results and on the class of  $1/f^\alpha$  noise distributions to which they are compared. Finally, we discuss our findings with regard to the relevant universality classes, and comment on questions brought up by our investigation, for which no clear answer seems available at the moment.

\*Electronic address: sldq@if.ufrj.br

## II. MODEL AND CALCULATIONAL METHOD

The single-interface model used here was introduced in Ref. 7 for the description of BN. We consider the adiabatic limit of a very slow driving rate, thus avalanches are considered to be instantaneous (occurring at a fixed value of the external field).

Simulations are performed on an  $L_x \times L_y \times \infty$  geometry, with the interface motion set along the infinite direction. The interface at time  $t$  is described by its height  $h_i \equiv h(x, y, t)$ , where  $(x, y)$  is the projection of site  $i$  over the cross-section. No overhangs are allowed, so  $h(x, y, t)$  is single-valued. We consider mainly  $L_y = 1$  (system dimensionality  $d = 2$ , interface dimensionality  $d' = d - 1 = 1$ ), and  $L_x = L_y$  ( $d = 3$ ,  $d' = 2$ ). For reasons to be explained below, we will use the following sets of boundary conditions: periodic (PBC), so every site has two neighbors for  $d = 2$  and four for  $d = 3$ ; free (FBC), meaning that the interface is horizontal at the edges ( $\partial h / \partial \hat{n} = 0$ , where  $\hat{n} = \hat{x}$  or  $\hat{y}$  is the normal in the cross-section plane), and mixed (MBC), i. e., periodic along  $x$  and free along  $y$ . These latter were employed in Ref. 10, to reproduce the physical picture of films with varying thickness.

Each element  $i$  of the interface experiences a force given by:

$$f_i = u(x, y, h_i) + k \sum_j [h_{\ell_j(i)} - h_i] + H_e , \quad (1)$$

where

$$H_e = H - \eta M . \quad (2)$$

The first term on the RHS of Eq. (1) is chosen randomly, for each lattice site  $\vec{r}_i \equiv (x, y, h_i)$ , from a Gaussian distribution of zero mean and standard deviation  $R$ , and represents quenched disorder. Large negative values of  $u$  lead to local interface pinning. The second term (where the force constant  $k$  is taken as the unit for  $f$ ) corresponds to elastic nearest-neighbor coupling (surface tension);  $\ell_j(i)$  is the position of the  $j$ -th nearest neighbor of site  $i$ . For MBC, sites at  $y = 1$  and  $y = L_y$  have only three neighbors on the  $xy$  plane (except in the monolayer case  $L_y = 1$  which is the two-dimensional limit, where all interface sites have two neighbors). The last term is the effective driving force, resulting from the applied uniform external field  $H$  and a demagnetizing field which is taken to be proportional to  $M = (1/L_x L_y) \sum_{i=1}^{L_x L_y} h_i$ , the magnetization (per site) of the previously flipped spins for a lattice of transverse area  $L_x L_y$ . For actual magnetic samples, the demagnetizing field is not necessarily uniform along the sample; even when it is (e.g. for a uniformly magnetized ellipsoid),  $\eta$  would depend on the system's aspect ratio [21]. Therefore, our approach amounts to a simplification, which is nevertheless expected to capture the essential aspects of the problem [9]. Here we use  $R = 5.0$ ,  $k = 1$ ,  $\eta = 0.05$ , values for which fairly broad distributions of avalanche sizes and roughness are

obtained [8, 9, 10]. We also consider the effects of taking  $\eta \equiv 0$ , i.e., the non-self-organizing limit.

We start the simulation with a flat wall. All spins above it are unflipped. The force  $f_i$  is calculated for each unflipped site along the interface, and each spin at a site with  $f_i \geq 0$  flips, causing the interface to move up one step. The magnetization is updated, and this process continues, with as many sweeps of the whole lattice as necessary, until  $f_i < 0$  for all sites, when the interface comes to a halt. The external field is then increased by the minimum amount needed to bring the most weakly pinned element to motion. The avalanche size corresponds to the number of spins flipped between two consecutive interface stops.

On account of the demagnetization term, the effective field  $H_e$  at first rises linearly with the applied field  $H$ , and then, upon further increase in  $H$ , saturates (apart from small fluctuations) at a value rather close to the critical external field for the corresponding model *without* demagnetization [7, 8]. The saturation  $H_e$  depends on  $R$ ,  $k$  and  $\eta$  (*not* noticeably on  $L_x$ ,  $L_y$ ) [8, 10], and can be found from small-lattice simulations. It takes  $10^2 - 10^3$  avalanches for a steady-state regime to be reached, as measured by the stabilization of  $H_e$  against  $H$ .

## III. ROUGHNESS DISTRIBUTIONS AND $1/f^\alpha$ NOISE

We have generated histograms of occurrence of interface roughness, to be examined in the context of universal fluctuation distributions [3, 4, 5, 6]. We have used only steady-state data, i.e., after the stabilization of  $H_e$  of Eq. (2) against external field  $H$ . This is the regime in which the system is self-regulated at the edge of criticality [7, 8]. As the model is supposed to mimic the data acquisition regime for BN, during which the external field grows linearly in time [7, 8, 9, 10, 15], the value of  $H$  is a measure of “time”.

At the end of each avalanche, we measured the roughness  $w_2$  of the instantaneous interface configuration at time  $t$ , as the (position-averaged) square width of the interface height [6, 22]:

$$w_2(t) = (L_x L_y)^{-1} \sum_{i=1}^{L_x L_y} (h_i(t) - \bar{h}(t))^2 , \quad (3)$$

where  $\bar{h}(t)$  is the average interface height at  $t$ . As the avalanches progress, one gets a sampling of successive equilibrium configurations; the ensemble of such configurations yields a distribution of the relative frequency of occurrence of  $w_2$ . Here we usually considered ensembles of  $5 \times 10^7$  events (one and a half orders of magnitude larger than in Ref. 10), so we ended up with rather clean distributions. This was essential, in order to resolve ambiguities left over from our previous results [10].

The width distributions for correlated systems at crit-

icity may be put into a scaling form [5, 6, 22, 23],

$$\Phi(z) = \langle w_2 \rangle P(w_2), \quad z \equiv w_2 / \langle w_2 \rangle, \quad (4)$$

where angular brackets stand for averages over the ensemble of successive interface configurations, and the size dependence appears only through the average width  $\langle w_2 \rangle$ . By running simulations with  $\mathcal{O}(10^6)$  events, and  $400 \leq L_x \leq 1200$  for  $d = 2$  ( $L_y = 1$ ),  $30 \leq L_x = L_y \leq 80$  for  $d = 3$  [10], we ascertained that Eq. (4) indeed holds, i.e., finite-size effects are not detectable in any significant way as far as the scaling functions  $\Phi(z)$  are concerned. The finite-size scaling of the first moment gives the roughness exponent [1]:

$$\langle w_2(L) \rangle \sim L^{2\zeta}, \quad (5)$$

In the context of critical fluctuation phenomena, it is known that boundary conditions have a non-trivial effect on scaling quantities, as infinite-range critical correlations are sensitive to the boundaries of the system [5, 6, 22, 24, 25]. This is the motivation for use of the assorted boundary conditions defined in Sec. II.

We have compared our results against the family of roughness distributions for  $1/f^\alpha$  noise, described in Refs. 6, 22. As explained there, such distributions are derived under the assumption that the Fourier modes into which the interface is decomposed are uncorrelated (generalized Gaussian approximation [22]), and with amplitudes such that the frequency dependence of the power spectrum is purely  $1/f^\alpha$  [6]. This is the simplest starting point from which one may expect non-trivial results (the trivial ones corresponding to the case in which the *real-space fluctuations* are themselves uncorrelated, implying  $\alpha = 1/2$ ).

## IV. RESULTS

### A. Influence of self-regulating term

We first investigated what could be learned about the relevance of the self-regulating term, as regards roughness distributions. In order to do so, we determined the approximate critical value  $H_e^c$  of the internal field  $H_e$  of Eq. (2), by starting a simulation with  $\eta \neq 0$  and waiting for  $H_e$  to stabilize. At that point, we set  $\eta = 0$  and repeatedly varied  $H$  in the interval  $(x H_e^c, H_e^c)$ ,  $x \lesssim 1$ , according to the procedure delineated in Sec. II. Though the interval of variation of  $H$  did affect the size distribution of avalanches, as this is what characterizes the proximity of the depinning point [7, 8], no change was apparent in the roughness data when comparing results, e.g., for  $x = 0.95$  and  $x = 0.9$ . For the simulations described in the remainder of this subsection, we used the latter value. In all cases studied, namely,  $d = 2$  PBC and  $d = 3$  with both MBC and PBC, the influence of the demagnetization term on the roughness PDFs is rather small, but systematic. This is illustrated in Fig. 1 for

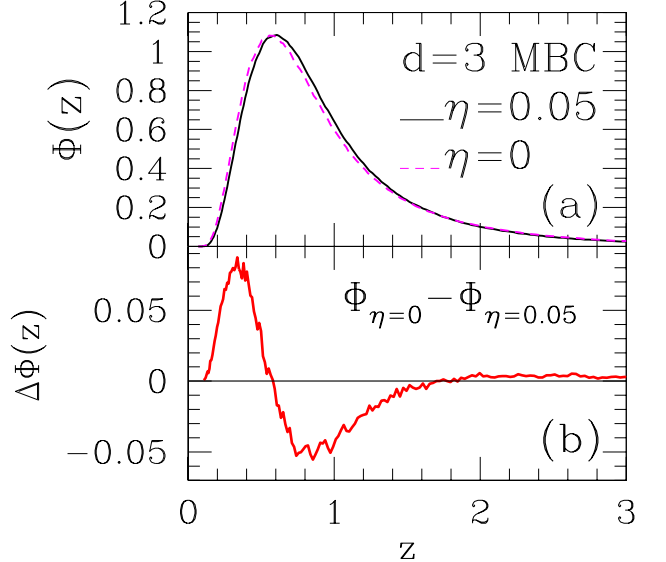


Figure 1: (a) Scaled probability distributions  $\Phi(z)$  in  $d = 3$  with MBC, for  $z$  defined in Eq. (4). Data for  $L = 40, 5 \times 10^7$  configurations. Full line: demagnetization factor  $\eta = 0.05$ ; dashed line:  $\eta = 0$ . (b) Scaling function difference against  $z$ .

$d = 3$  with MBC, the case for which the deviations between the  $\eta \neq 0$  and  $\eta = 0$  sets of data are the largest in magnitude. One sees that neglecting the demagnetizing term causes a small leftward shift of the scaling curve. As we will see in Section IV B, the changes it causes to the fits of our distributions to the analytical  $1/f^\alpha$  curves are of the order of systematic imprecisions characteristic of the fitting procedure. Nevertheless, it is instructive to seek the physical origins of such effect. This is done by direct inspection of the unscaled PDFs. In Fig. 2 it is apparent that, for  $\eta = 0$  the high-end tail of  $P(w_2)$  is slightly fatter than for  $\eta \neq 0$ , at the expense of a small amount of depletion around the most probable value of  $w_2$ . Accordingly, the average  $\langle w_2 \rangle$  is higher by  $\simeq 8\%$  in the former case than in the latter (the fractional difference between averages is the same also for  $d = 2$  and  $d = 3$  PBC). Such a trend can be understood by recalling that the  $\eta = 0$  data have been collected just *below* the depinning transition, i.e., still within the regime where pinning forces are dominant. Thus the interface mostly meanders about, in order to comply with local energy minimization requests. The complement of this picture is that, for  $H > H_c$  the interface moves with finite speed, more or less ignoring local randomness configurations, and becoming smoother the farther one is above the critical point. In short, for a given lattice size the average interface roughness decreases monotonically as the external field (driving force) is increased across its critical value.

The interpretation of the small differences between  $\eta =$

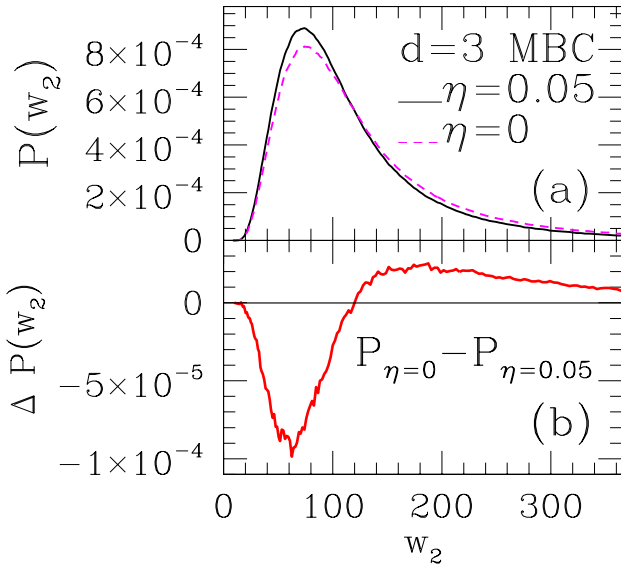


Figure 2: (a) Probability distributions  $P(w_2)$  in  $d = 3$  with MBC. Data for  $L = 40, 5 \times 10^7$  configurations. Full line: demagnetization factor  $\eta = 0.05$ ; dashed line:  $\eta = 0$ . (b) Probability distribution difference against  $w_2$ . Extent of horizontal axis corresponds to the same interval of  $z$ -variation in Fig. 1.

0 and  $\eta \neq 0$  distributions is then as follows: (i) because of the way in which data for the former were collected here, they represent a system just below  $H_c$ , for which interface roughness is slightly larger than at the critical point; and (ii) the closeness of  $\eta = 0$  data to those for  $\eta \neq 0$ , and the way in which both sets of data differ, strongly suggest that behavior *at* the critical point of the  $\eta = 0$  system is the same as that of the  $\eta \neq 0$  (self-regulated) case. We conclude that the self-regulating term is irrelevant, as far as critical roughness distributions are concerned.

### B. PBC, $d = 2$ and 3

Analytical expressions for the  $1/f^\alpha$  distributions with PBC are either given in Ref. 6 ( $d = 2$ ), or can be derived straightforwardly from Refs. 6, 22 ( $d = 3$ ). In the latter case, the use of exact identities for two-dimensional lattice sums [26] speeds up calculations considerably. Estimates of the exponent  $\zeta$  of Eq. (5), from power-law fits of simulational data with  $\mathcal{O}(10^6)$  events, and  $400 \leq L_x \leq 1200$  for  $d = 2$ ,  $30 \leq L \leq 80$  for  $d = 3$ , give  $\zeta(2d, \text{PBC}) = 1.24(1)$ ,  $\zeta(d = 3, \text{PBC}) = 0.71(1)$  [10].

Consideration of the scaling properties of height-height correlation functions and their Fourier transforms then suggests [22], for the generalized Gaussian case of independent Fourier modes, that

$$\alpha = d' + 2\zeta \quad (d' = d - 1), \quad (6)$$

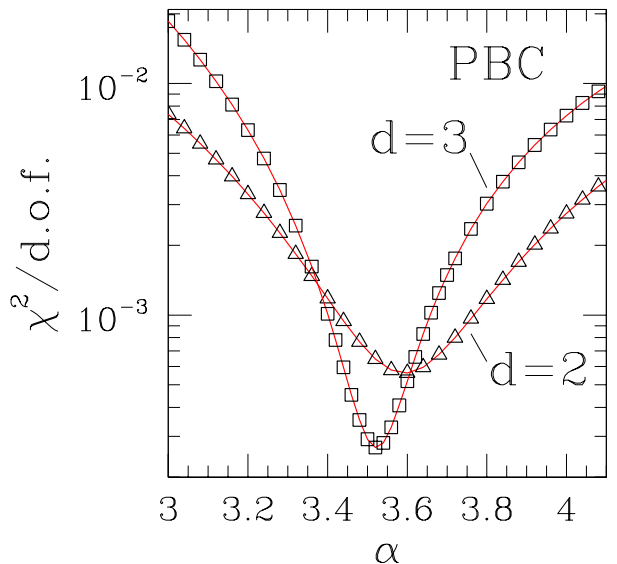


Figure 3:  $\chi^2$  per degree of freedom ( $\chi^2/\text{d.o.f.}$ ) for fits of simulation data with PBC to analytical forms of  $1/f^\alpha$  distributions, against  $\alpha$ . Triangles:  $d = 2$ ,  $L_x = 400$ ; squares,  $d = 3$ ,  $L = 40$ .

which would imply  $\alpha = 3.48(2)$  ( $d = 2$ ),  $3.42(2)$  ( $d = 3$ ).

Such predictions can be quantitatively checked by estimating the values of  $\chi^2$  per degree of freedom ( $\chi^2/\text{d.o.f.}$ ) from fits of our simulation results to the analytical distributions. Since, even with  $5 \times 10^7$  samples, the simulational data eventually get frayed at the top end, given the long forward tails characteristic of all systems studied here, our fits used only data for which  $\Phi(z) \geq 10^{-3}$ . This turned out not to be a drastic restriction, as we were left typically with  $100 - 200$  points to fit in each case. Assuming the uncertainty in the value of  $\alpha$  that best fits our data to be given by requiring that  $\chi^2/\text{d.o.f.}$  stay within 150% of its minimum, we quote from the data shown in Fig. 3:  $\alpha = 3.60(13)$  ( $d = 2$ );  $3.52(6)$  ( $d = 3$ ). The agreement with the above predictions is satisfactory, though slight discrepancies remain. A visual check of the goodness-of-fit for each case is given in Figs. 4 and 5.

Fitting  $\eta = 0$  data to the closed-form distributions produces curves whose minima of  $\chi^2/\text{d.o.f.}$  are essentially the same as in Fig. 3, and slightly shifted rightwards. Using the same criteria as above for the estimation of error bars, we have, for  $\eta = 0$ :  $\alpha = 3.64(16)$  ( $d = 2$ );  $3.59(5)$  ( $d = 3$ ).

Detailed discussion, and pertinent comparisons with data from Ref. 22, will be deferred to Section V.

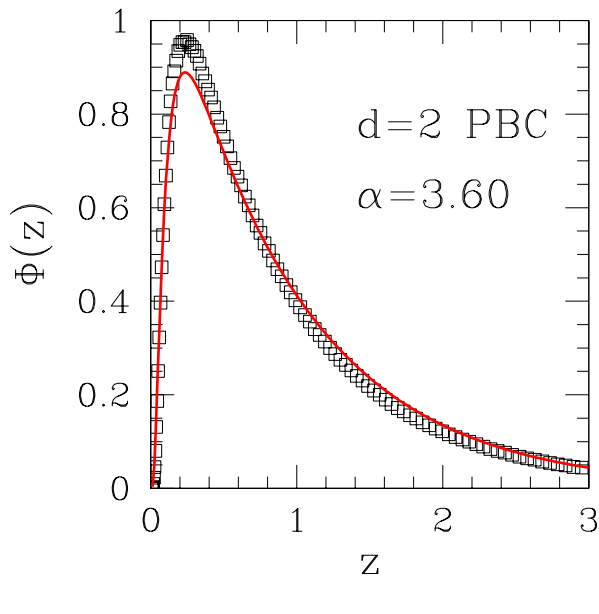


Figure 4: Scaled probability distribution  $\Phi(z)$  in  $d = 2$  (PBC), for  $z$  defined in Eq. (4), from  $5 \times 10^7$  configurations. Squares: simulation data ( $L = 400$ ). Full line is roughness distribution for  $1/f^\alpha$  noise given in Ref. 6, with  $\alpha = 3.60$ .

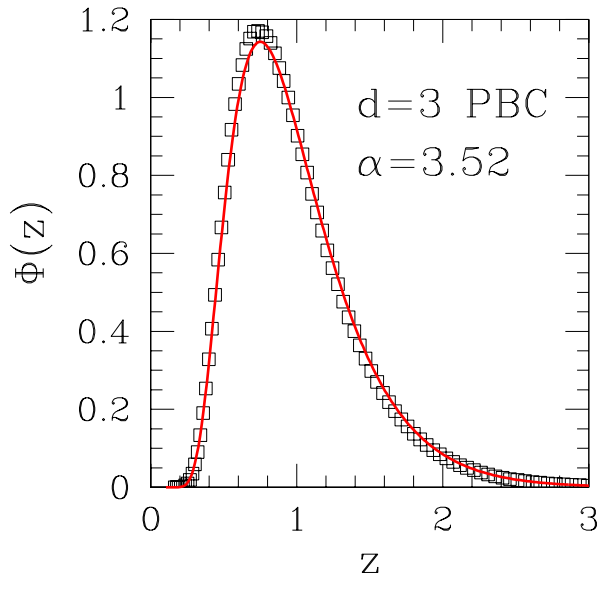


Figure 5: Scaled probability distribution  $\Phi(z)$  in  $d = 3$  with PBC, for  $z$  defined in Eq. (4), from  $5 \times 10^7$  configurations. Squares: simulation data ( $L = 40$ ). Full line is roughness distribution for  $1/f^\alpha$  noise, with  $\alpha = 3.52$ .

### C. FBC, $d = 2$ and 3

We have generated roughness data in both  $d = 2$  and 3 with FBC. Similarly to the PBC cases, estimates of the exponent  $\zeta$  of Eq. (5) were extracted from power-law fits of simulational data with  $\mathcal{O}(10^6)$  events, and  $400 \leq L_x \leq 1000$  for  $d = 2$ ,  $30 \leq L \leq 80$  for  $d = 3$ . The results are  $\zeta(2d, \text{FBC}) = 1.28(2)$ ,  $\zeta(d = 3, \text{FBC}) = 0.89(1)$ . While the former value may be construed as not inconsistent with PBC and FBC giving the same universality class for  $d = 2$ , the same picture cannot hold for  $d = 3$ . This latter case is not surprising, since past experience [5, 6, 22, 24, 25] indicates that boundary conditions do have significant influence on scaling functions of critical systems. In order to get further insight, we turn to the roughness PDFs.

We first recall the effect of FBC on  $1/f^\alpha$  distributions. The generating function  $G(s) = \int dw_2 P(w_2) e^{-sw_2}$  has the general form for PBC [6, 22]

$$G_p(s) = \prod_{\mathbf{n} \neq 0} \left(1 + \frac{s}{\mathbf{n}^\alpha}\right)^{-1/2}, \quad (7)$$

where  $\mathbf{n}$  is a lattice vector in  $d - 1$  dimensions with integer coordinates. Because all  $\mathbf{n}$  are counted, the square root disappears due to the (at least) twofold degeneracy. Requiring that the interface be horizontal at the edges implies that the Fourier representation of  $h(t)$  includes only cosines. The corresponding  $G_f(s)$  has the degeneracy of its singularities cut in half, compared to PBC.

In  $d = 2$ , this means that the single poles found for PBC turn into square-root singularities. Evaluation of  $P(w_2)$  as the inverse Laplace transform of  $G_f(s)$ , via the residue theorem, then appears to be unfeasible in general, though the special case  $\alpha = 2$  can be tackled [6]. Therefore, we are not able to perform a minimization of  $\chi^2/\text{d.o.f}$  as a function of  $\alpha$ , similar to that of Section IV B above. For completeness, our simulational data are displayed in Fig. 6, together with those for PBC for comparison. The inset of the Figure shows the tails of both distributions on a semi-logarithmic scale. One sees that neither case is a pure exponential, and that decay of FBC data is significantly slower than that for PBC.

Turning to  $d = 3$ , all poles of  $G_p(s)$  have even degeneracy. A straightforward adaptation for FBC is as follows. Recalling that the lattice sums  $\sum_{\mathbf{n}} |\mathbf{n}|^{-\alpha}$  which crop up in the calculation of  $\langle w_2 \rangle$  [5, 6, 27] must be halved, this implies a rescaling of the variable  $s$ , so formally one can write [6]:

$$G_f(s) = \sqrt{G_p(2s)}. \quad (8)$$

Our data, and the results of their fitting to the analytical distribution functions obtained with help of Eq. (8), are shown in Fig. 7. The above-quoted value  $\zeta = 0.89(1)$ , from the finite-size scaling of  $\langle w_2 \rangle$ , together with Eq. (6), would suggest  $\alpha = 3.78(2)$ . However, as shown in the inset of the Figure, examination of the dependence of  $\chi^2/\text{d.o.f.}$  against  $\alpha$  shows a clear minimum at  $\alpha = 3.18(8)$

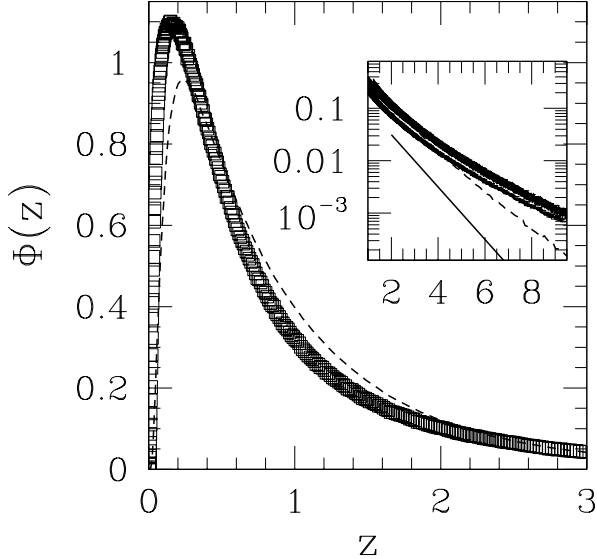


Figure 6: Scaled probability distribution  $\Phi(z)$  in  $d = 2$ , for  $z$  defined in Eq. (4), from  $5 \times 10^7$  configurations. All are simulation data ( $L = 400$ ). Squares: FBC. Dashed line: PBC. Inset: same variables as on main diagram, but with logarithmic scale on the vertical axis, showing large- $z$  data. Full line: pure exponential decay, for comparison.

(error bars estimated as in Section IV B); data for  $3.6 \leq \alpha \leq 4$  (not shown) give no indication of a second minimum. As can be seen in the main Figure, the  $\alpha = 3.18$  curve indeed appears closer to the data than that for  $\alpha = 3.78$ , though noticeable discrepancies remain.

#### D. MBC, $d = 3$

Estimates of the exponent  $\zeta$  of Eq. (5) were again extracted from power-law fits of simulational data with  $\mathcal{O}(10^6)$  events, and  $30 \leq L \leq 80$  for  $d = 3$  MBC, with the result  $\zeta(d = 3, \text{MBC}) = 0.87(1)$  [10].

The Fourier representation of  $h(t)$  with MBC can be put in the form:

$$h(x, y) = \sum_{m,n} c_{mn} e^{2\pi i (mx + \frac{n}{2}y)/L}, \quad (9)$$

where  $m, n = 0, \pm 1, \pm 2, \dots$ ,  $(m, n) \neq (0, 0)$ , and  $c_{-m,n} = c_{m,n}^*$ ;  $c_{m,-n} = c_{m,n}$ . Thus a global rescaling such as that of Eq. (8) is not possible. On the other hand, starting from Eq. (9), an analysis similar to that of Refs. 6, 27 suggests a generating function:

$$G_m(s) = \prod_{m,n} \left( 1 + \frac{s}{(4m^2 + n^2)^{\alpha/2}} \right)^{-1/2}, \quad (10)$$

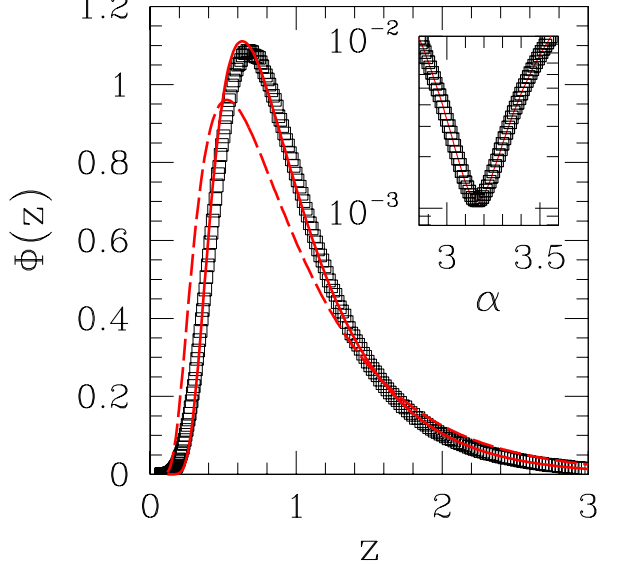


Figure 7: Scaled probability distribution  $\Phi(z)$  in  $d = 3$  with FBC, for  $z$  defined in Eq. (4), from  $5 \times 10^7$  configurations. Squares: simulation data ( $L = 40$ ). Lines are roughness distribution for  $1/f^\alpha$  noise, with  $\alpha = 3.18$  (full) and  $3.78$  (dashed). Inset:  $\chi^2/\text{d.o.f.}$  against  $\alpha$ , for fits of simulation data against  $1/f^\alpha$  distributions, showing a minimum at  $\alpha = 3.18$ .

again with  $(m, n) \neq (0, 0)$ . The double sum  $\sum_{m,n} (4m^2 + n^2)^{-\alpha/2}$ , which appears in the subsequent expression for  $\langle w_2 \rangle$ , corresponds to  $\mathcal{Q}(1, 0, 4)$  of Ref. 26 and can be easily evaluated.

We have performed fits of simulational data to the closed-form PDFs calculated as above, with results displayed in Fig. 8. While Eq. (6), with  $\zeta = 0.87(1)$ , gives  $\alpha = 3.74(2)$ , the minimum of  $\chi^2/\text{d.o.f.}$  (see inset) indicates  $\alpha = 3.36(10)$ . The overall quality of fits is slightly worse than for  $d = 3$  FBC (refer to Fig. 7).

## V. DISCUSSION AND CONCLUSIONS

We begin our discussion by recalling from Ref. 10 and Sec. IV B that, for the model considered here with PBC, the finite-size scaling of the first moment of the distribution gives  $\zeta(2d, \text{PBC}) = 1.24(1)$ ,  $\zeta(d = 3, \text{PBC}) = 0.71(1)$ . Both compare well with the usually accepted values for the quenched Edwards-Wilkinson (EW) universality class [11, 12, 13, 14], respectively  $\zeta \simeq 1.25$  ( $d = 2$ ) and  $\zeta \simeq 0.75$  ( $d = 3$ ). Furthermore, consideration of the full distributions points the same way: our simulational data displayed in Figs. 4 and 5 match very well those in Figure 2 of Ref. 22 which concern the EW model. The agreement with EW behavior is consistent with our results of Sec. IV A regarding the independence of scaled roughness distributions on the demagnetizing

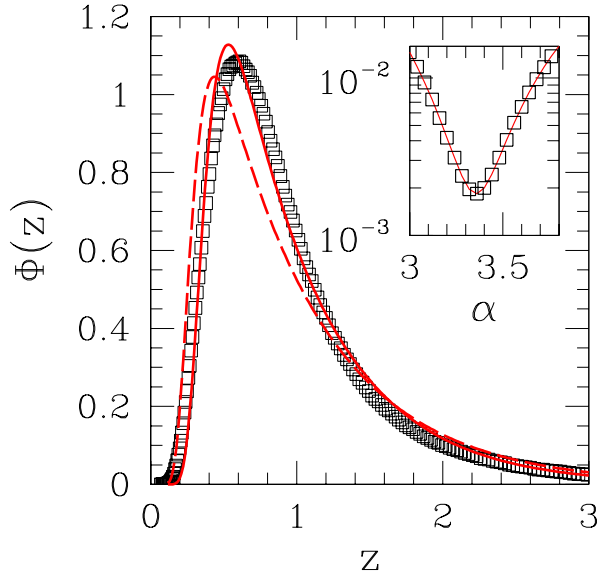


Figure 8: Scaled probability distribution  $\Phi(z)$  in  $d = 3$  with MBC, for  $z$  defined in Eq. (4), from  $5 \times 10^7$  configurations. Squares: simulation data ( $L = 40$ ). Lines are roughness distribution for  $1/f^\alpha$  noise, with  $\alpha = 3.36$  (full) and  $3.74$  (dashed). Inset:  $\chi^2/\text{d.o.f.}$  against  $\alpha$ , for fits of simulation data against  $1/f^\alpha$  distributions, showing a minimum at  $\alpha = 3.36$ .

term. Indeed, the quenched EW equation can be written as [14]

$$\frac{\partial h(\mathbf{x}, t)}{\partial t} = u(\mathbf{x}, h) + a \nabla^2 h(\mathbf{x}) + f, \quad (11)$$

where  $u$  represents quenched disorder and  $f$  is the external driving force. This has a one-to-one correspondence with Eq. (1), except that in that Equation we allowed for the self-regulating, demagnetizing, term. Having shown that such mechanism is irrelevant as far as scaled roughness distributions are concerned, it becomes tenable to assume that, overall, our model belongs to the EW universality class.

Still for PBC, the connection between the exponents  $\alpha$  and  $\zeta$ , predicted [22] in Eq. (6), is verified within reasonable error bars. On the other hand, for both FBC and MBC our results are not conducive to the same conclusion. We briefly examine some possible causes for this disagreement.

(i) The generalizations summarized respectively in Eq. (8) for FBC, and in Eqs. (9) and (10) for MBC, are somehow at fault. While this possibility cannot be discarded at the outset, alternative forms would then have to be produced and compared to our data.

(ii) Eq. (6) does not hold for boundary conditions other than PBC. This is unlikely, since that Equation was derived for generalized Gaussian distributions [22] with the only assumption that the large-scale behavior is determined by a single observable. If this works for PBC, then it should do so for FBC or MBC as well.

(iii) The generalized Gaussian distributions for  $1/f^\alpha$  noise are not strictly suitable for this case. Indeed, it is known that, even for PBC, small but systematic discrepancies remain for generalized depinning problems, whose origins can be traced to higher cumulants of the correlation functions [22]. Thus, in this sense the  $1/f^\alpha$  distributions are not expected to be a perfect fit; comparison of our PBC results on the one hand, and those for FBC and MBC on the other, suggests that, if this is the explanation, then the corrections for the latter cases have significantly larger amplitude than for the former.

Clearly, more work is needed in order to clarify the picture, as regards the connection between  $1/f^\alpha$  distributions and generalized depinning transitions.

## Acknowledgments

The author thanks Tibor Antal and Zoltán Rácz for their advice on numerical evaluation of the closed-form PDFs, as well as Robin Stinchcombe and J. A. Castro for interesting discussions and suggestions. This research was partially supported by the Brazilian agencies CNPq (Grant No. 30.0003/2003-0), FAPERJ (Grant No. E26-152.195/2002), FUJB-UFRJ and Instituto do Milênio de Nanociências-CNPq.

---

[1] A.-L. Barabási and H. E. Stanley, *Fractal Concepts in Surface Growth* (Cambridge University Press, Cambridge, 1995).  
[2] M. Kardar, Phys. Rep. **301**, 85 (1998).  
[3] S. T. Bramwell, P. C. W. Holdsworth, and J.-F. Pinton, Nature (London) **396**, 552 (1998).  
[4] S. T. Bramwell, K. Christensen, J.-Y. Fortin, P. C. W. Holdsworth, H. J. Jensen, S. Lise, J. M. López, M. Nicodemi, J.-F. Pinton, and M. Sellitto, Phys. Rev. Lett. **84**, 3744 (2000).  
[5] T. Antal, M. Droz, G. Györgyi, and Z. Rácz, Phys. Rev. Lett. **87**, 240601 (2001).  
[6] T. Antal, M. Droz, G. Györgyi, and Z. Rácz, Phys. Rev. E **65**, 046140 (2002).  
[7] J. S. Urbach, R. C. Madison, and J. T. Markert, Phys. Rev. Lett. **75**, 276 (1995).  
[8] M. Bahiana, B. Koiller, S. L. A. de Queiroz, J. C. Denardin, and R. L. Sommer, Phys. Rev. E **59**, 3884 (1999).  
[9] S. L. A. de Queiroz and M. Bahiana, Phys. Rev. E **64**, 066127 (2001).  
[10] S. L. A. de Queiroz, Phys. Rev. E **69**, 026126 (2004).  
[11] H. Leschhorn, Physica A **195**, 324 (1993).  
[12] H. A. Makse and L. A. N. Amaral, Europhys. Lett. **31**,

379 (1995).

[13] H. A. Makse, S. Buldyrev, H. Leschhorn, and H. E. Stanley, *Europhys. Lett.* **41**, 251 (1998).

[14] A. Rosso, A. K. Hartmann, and W. Krauth, *Phys. Rev. E* **67**, 021602 (2003).

[15] G. Durin and S. Zapperi, e-print cond-mat 0404512.

[16] E. Puppin, *Phys. Rev. Lett.* **84**, 5415 (2000).

[17] D.-H. Kim, S.-B. Choe, and S.-C. Shin, *Phys. Rev. Lett.* **90**, 087203 (2003).

[18] K. L. Babcock and R. M. Westervelt, *Phys. Rev. Lett.* **64**, 2168 (1990).

[19] P. J. Cote and L. V. Meisel, *Phys. Rev. Lett.* **67**, 1334 (1991).

[20] K. P. O'Brien and M. B. Weissman, *Phys. Rev. E* **50**, 3446 (1994).

[21] S. Zapperi, P. Cizeau, G. Durin, and H. E. Stanley, *Phys. Rev. B* **58**, 6353 (1998).

[22] A. Rosso, W. Krauth, P. LeDoussal, J. Vannimenus, and K. J. Wiese, *Phys. Rev. E* **68**, 036128 (2003).

[23] G. Foltin, K. Oerding, Z. Rácz, R. L. Workman, and R. K. P. Zia, *Phys. Rev. E* **50**, R639 (1994).

[24] T. Antal, M. Droz, and Z. Rácz, *J. Phys. A* **37**, 1465 (2004).

[25] K. Binder, *Z. Phys. B* **43**, 119 (1981).

[26] I. J. Zucker and M. M. Robertson, *J. Phys. A* **8**, 874 (1975).

[27] Z. Rácz and M. Plischke, *Phys. Rev. E* **50**, 3530 (1994).